JOURNAL OF SPACECRAFT AND ROCKETS
Vol. 45, No. 3, May–June 2008

Ballute Entry Systems for Lunar Return and Low-Earth-Orbit Return Missions

Ian G. Clark* and Robert D. Braun†
Georgia Institute of Technology, Atlanta, Georgia 30332-0150

DOI: 10.2514/1.31612

This study investigates the feasibility of using ballutes for Earth entry at both lunar- and low-Earth-orbit return velocities. Multiple entry strategies were investigated using analysis methods suitable for conceptual design and assuming an Apollo-derived entry vehicle. Primary ballute size drivers are the thermal limitations and areal densities of the ballute material. Lunar-return entries that jettison the ballute after achieving low-Earth-orbit conditions were shown to reduce heating rates to within reusable thermal protection system limits. Deceleration was mitigated to approximately 4 *g* along a lunar-return trajectory when a moderate amount of lift was applied subsequent to ballute jettison. Investigation of a lower mass lunar-return cargo variant of the Crew Exploration Vehicle was shown to reduce ballute system mass and size. Ballute system mass as a percentage of the total entry mass was shown to be relatively independent of the entry mass for the range of lunar-return missions evaluated. However, material requirements indicate that continued technology development may be required for lunar-return system viability. Missions aimed at augmenting existing systems to provide downmass capability from the International Space Station showed promising results in terms of entry loads, required material areal densities, and ballute system mass and size.

Nomenclature

A_b	=	ballute surface area, m^2
C_D	=	drag coefficient
C_p	=	pressure coefficient
D_b	=	ballute diameter, m
D_c	=	diameter of entry vehicle, m
g_0	=	gravitation acceleration on Earth surface, m/s^2
Kn	=	Knudsen number
L/D	=	lift to drag ratio
m	=	mass, kg
q_∞	=	dynamic pressure, Pa
R	=	specific gas constant
R_n	=	nose radius of entry vehicle, m
R_t	=	radius of ballute minor torus, m
R'_t	=	distance from centerline of ballute to minor torus center, m
s	=	molecular speed ratio
T_∞	=	ambient atmospheric temperature, K
T_w	=	wall temperature, K
V_∞	=	vehicle velocity, m/s
y	=	dummy integration variable
β_b	=	ballute ballistic coefficient
γ	=	flight-path angle, deg
Δp	=	pressure differential, Pa
θ	=	inclination to freestream, deg
θ_b	=	ballute half-cone angle, deg
σ_N	=	normal accommodation coefficient
σ_T	=	tangential accommodation coefficient
ϕ_{tank}	=	tank-mass factor, m

Presented as Paper 6276 at the AIAA Atmospheric Flight Mechanics Conference and Exposition, Keystone, CO, 21–24 August 2006; received 19 June 2007; revision received 17 October 2007; accepted for publication 13 November 2007.

*Graduate Research Assistant, Guggenheim School of Aerospace Engineering. Student Member AIAA.

†Associate Professor, Guggenheim School of Aerospace Engineering. AIAA Fellow.

I. Introduction

THE problem of Earth return from the moon can be summarized as the requirement to dissipate the large amount of kinetic energy associated with an entry vehicle on a lunar-return trajectory. Common approaches to this problem are to use the aerodynamics of the entry vehicle to decelerate in a controlled process and/or to tailor the entry trajectory so as to dissipate energy in a benign manner. For the former approach, direct application of drag requires the entry vehicle to reach an appreciable level of atmospheric density, which increases the heat rate and magnitude of deceleration felt by the vehicle. Whereas deceleration at higher altitudes and lower densities is preferable, constraints on vehicle shape and size may not allow for the large drag coefficients and reference areas required. However, reference area can be drastically altered through the use of an inflatable hypersonic drag device commonly termed a ballute. Through an increase in reference area, a ballute provides several advantages during planetary entry and descent. By achieving improved deceleration at lower atmospheric densities, the heating rates encountered can be significantly lessened. A large ballute also serves to increase the effective nose radius of the entry vehicle, providing further reduction in the convective heat rate, though with the potential of increasing the radiative heat rate. Additionally, a ballute can expand an available entry corridor by preventing skipout at shallower flight-path angles. These benefits have the potential to improve the mass fraction devoted to a vehicle's entry system by reducing the required heat shield mass and improving the payload volume fraction. Ballute technology may also provide a reasonable alternative for cases in which thermal protection systems are not yet qualified or where elimination of thermal protection system failure modes is desired.

First theorized in the early 1960s, ballutes (from the contraction of balloon and parachute) have long been envisioned for a variety of mission concepts, including aerocapture at Mars [1] or Saturn's moon Titan [2]. More recently, emphasis has been placed on maturing the designs and technologies associated with deployable systems. Toward this end, flight demonstrations such as the inflatable reentry and descent technology (IRDT-1) mission [3] and the upcoming inflatable reentry vehicle experiment (IRVE) mission [4] have sought to characterize the behavior of ballutes under reentry conditions. For a more extensive history, the reader is directed to the survey paper by Rohrschneider and Braun [5].

Entering the Earth's atmosphere from a lunar-return trajectory is one of the more difficult tasks facing future human exploration. With entry velocities roughly 40% higher than a typical entry from low

Earth orbit, constraints on vehicle heating and deceleration drive vehicle design. During the Apollo program, reentry of the command module at 11 km/s resulted in peak heat rates between 250 and 300 W/cm^2 and a peak deceleration of over 7 g [6]. The currently envisioned Earth return vehicle, the crew exploration vehicle (CEV), will be larger and heavier than the Apollo command module and consequently will encounter more sever conditions upon Earth reentry. The CEV is being designed to tolerate a peak heat rate on the order of 1000 W/cm^2 [7]. The high heating rates encountered by the Apollo command module dictated the use of an ablative thermal protection system (TPS). Although ablative systems are frequently used in robotic exploration missions, the original production line for the ablative material used by the Apollo program, AVCOAT, was shut down for several decades [8] and, thus, a new material needs to be developed or an existing material recertified for use at these conditions on human exploration missions. Given that both of these options represent potential risk and significant investment, an alternative technology path consisting of ballute-based entry may merit parallel investigation. Such a system has the potential to mitigate heating rates sufficiently, reducing the mass and performance requirements of the ablative TPS, or allow for the use of an already developed reusable TPS concept. While mitigating or eliminating TPS failure modes, a ballute system is not without its own development complexity and risk.

In addition to lunar-return missions, another near-term mission in which ballutes may provide an advantage is the safe return of cargo from the International Space Station (ISS) to Earth. At present, there are three means of access to the space station: the space shuttle, the Russian progress resupply vehicles, and the Russian Soyuz spacecraft, and, of those, only the space shuttle and Soyuz are designed for Earth reentry. With the looming retirement of the space shuttle (currently forecast for the 2010 timeframe), the capacity to safely return mass from the ISS will be dramatically reduced. Though the potential exists for continued use of the Soyuz, the downmass capabilities of the Soyuz are likely insufficient to meet the forecasted requirements of 1–11 t per year. Additional means of cargo delivery to the International Space Station are in development in the form of government sponsored vehicles such as the European automated transfer vehicle (ATV) and the Japanese H-II transfer vehicle (HTV). However, neither of these vehicles are intended to survive Earth reentry and thus cannot provide a downmass capability. Commercial cargo delivery services are also being solicited as part of NASA's Commercial Orbital Transportation Services (COTS) effort [9]. Concepts associated with the COTS effort are still in the design stages and significant effort remains before an initial operating capability. A logical alternative would be to modify one of the current stable of cargo upmass vehicles with the capability to survive the entry environment. The addition of a ballute to one of these resupply vehicles may allow for vehicle survivability and thus eliminate the need to further develop a dedicated downmass cargo vehicle.

The focus of this paper is to assess the feasibility of using a ballute for near-term exploration missions. These include a human exploration vehicle returning on a lunar trajectory, cargo return from the moon, and cargo return from low Earth orbit. The assessment is performed by first quantifying the impacts that a ballute can have on reference trajectories with regard to heating and deceleration, and subsequently sizing the ballute entry system. This study also explores different deployment strategies for using a ballute, including an early jettison of the ballute after a predefined velocity decrement. Trends are explored that can assist in determining the performance metrics of a ballute entry system. As the impetus for this study is the Vision for Space Exploration, emphasis is placed on the performance augmentation that a ballute entry system could provide to the baseline CEV.

II. Approach

The study was broken into two phases with the first seeking to quantify the advantages ballutes can offer during entry and the second seeking to investigate sizing trends of ballutes. The first phase consisted of running a broad range of entry trajectories over a variety of ballute sizes and quantifying the magnitude and profile of deceleration, the heat rate profile, and the dynamic pressure experienced by both the ballute and the CEV. The trajectories were run using multiple entry strategies. The initial strategy consisted of using the ballute from atmospheric entry through subsonic conditions. An alternative strategy investigated for lunar-return missions is a hybrid direct-entry approach where the ballute is used to impart a sufficient velocity decrement such that the remainder of the entry is aerothermodynamically equivalent to entry from low Earth orbit [10]. That is, the ballute is used to decelerate the CEV to low-Earth-orbit (LEO) velocities ($\sim$7.8 km/s) and is subsequently jettisoned. It should be noted that this strategy applies equally to continued entry of the CEV or to an aerocapture of this system into LEO for ISS rendezvous or a subsequent deorbit. The potential advantages of this approach include reducing the heating and pressure loads on the ballute while mitigating the heating and deceleration profiles seen by the CEV to those consistent with initial plans for the LEO version of the CEV (Block I) [11]. Within this approach, two postjettison CEV entries were investigated: an operationally simple ballistic CEV entry and a low-L/D lifting CEV entry. Although the study focused primarily on a crewed entry vehicle for lunar return, investigations into a lower mass cargo variant of the lunar CEV were also performed.

Portions of the study examining the ISS downmass were performed using the European ATV as the baseline vehicle. Only a simple, no-jettison entry strategy was examined, as entry loads from LEO are considerably less than those from a lunar return.

A. Configuration

To assist in evaluating a large number of configurations, entry trajectories, and deployment strategies, analysis methods suited for conceptual design were used. The results attained in this investigation focus on the feasibility of a ballute system at the conceptual design level and, as such, do not seek to offer quantitative validation that the concepts explored are feasible in regard to higher level analyses, e.g., aeroelastic [12] and structural dynamic response [13].

A lunar-return entry vehicle configuration was selected consistent with the CEV design chosen by NASA's Exploration Systems Architecture Study (ESAS) [11]. In particular, the vehicle's shape is based on the Apollo command module with a 5.5 m base diameter. Other major dimensions are presented in Fig. 1. The nose radius was linearly scaled as well from an Apollo value of 4.6 m to a new value of 6.4 m. Lastly, the mass of the crewed entry vehicle was kept fixed at 9500 kg, the ESAS-estimated mass of the lunar variant of the CEV. Subsequent analyses examining a cargo variant of the lunar CEV kept the vehicle dimensions the same, but varied the entry mass from 2000 to 9000 kg. The baseline LEO cargo vehicle incorporated a 4.48 m diameter and assumed a nose radius of 5.21 m, derived from ATV dimensions [14]. The dimensions of the LEO cargo vehicle were kept constant over a range of entry masses from 1 to 20 t.

Though many ballute mission profiles have been previously studied, a majority focus on three distinct ballute configurations, shown in Fig. 2. The trailing torus design consists of an inflated ring

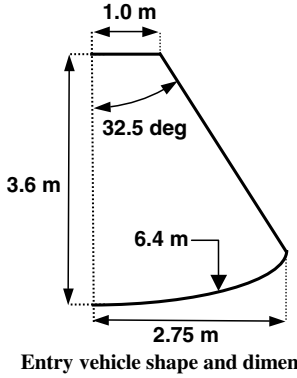

Fig. 1 Entry vehicle shape and dimensions.

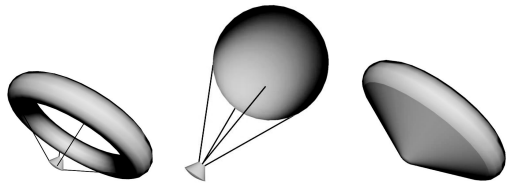

Fig. 2 Ballute configurations: a) trailing torus, b) trailing sphere, and c) clamped torus.

that is attached to the entry vehicle by a series of tethers. The trailing sphere is of a similar nature, though it replaces the torus shape with a simple sphere. The clamped torus does away with tethers and instead attaches the torus to the entry vehicle with a conical frustum that fully encloses the vehicle.

A ballute's capacity to decelerate the entry vehicle can be measured by its drag area. The drag produced by the ballute must in turn be balanced by the relative mass contribution of the ballute. That is, a large trailing sphere may produce as much drag as a medium-sized clamped torus; however, the trailing sphere may require less material and pressurant, and therefore be less massive. Assuming that the majority of the ballute system's mass comes from the ballute material, then a first-order means of comparing ballute types is through use of a ballute ballistic coefficient β_b. Conventionally, the ballistic coefficient is calculated as the ratio of a vehicle's mass to its drag contribution. If one were to assume that a majority of a ballute system's mass is from the ballute itself, and not from secondary sources such as the inflation system, than an alternative representation of ballistic coefficient could be defined using the surface area of a given concept. That is, two ballute concepts having the same surface area should have approximately the same mass. As such, the ballute ballistic coefficient can be defined as follows.

$$\beta_b = \frac{A_b}{C_D A_{\text{ref}}} \tag{1}$$

Using this dimensionless form of the ballistic coefficient, if two ballutes have the same total surface area, and thus roughly the same mass, the one with the lower value of the ballute ballistic coefficient would produce a greater degree of drag and deceleration. Thus, a lower value of β_b is typically favored as it represents a more effective ballute. The respective values of β_b for the three ballute types are summarized in Table 1.

The notation used for defining the dimensions of the trailing and clamped torus ballutes is presented in Fig. 3. Note that in the calculation of C_D and β_b, the reference area, A_{ref}, is computed using Eq. (2).

$$A_{\text{ref}} = \pi R_b^2 \tag{2}$$

The hypersonic drag coefficients listed in Table 1 are calculated from Newtonian aerodynamics. From Table 1, it can be seen that the advantage the trailing torus provides in reduced surface area vs the clamped version is insufficient to overcome its significantly lower drag contribution. Of the three ballute types, the trailing sphere is calculated as having the lowest β_b.

Though ballutes are often considered solely for their drag characteristics, the clamped configuration offers advantages in the heating regime as well. Because of the separation distance between the towed ballute and its entry vehicle, the ballute can be exposed to adverse entry vehicle wake effects. Previous studies focusing on

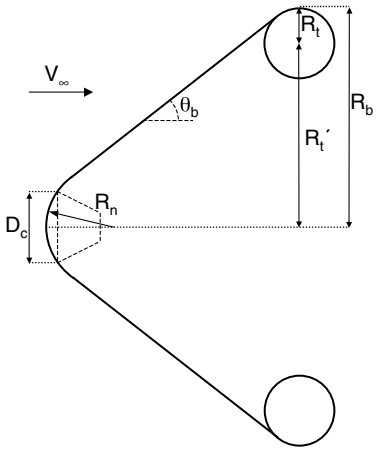

Fig. 3 Toroidal ballute geometry definitions.

these effects noted several vehicle/ballute behaviors, including the possibility of unfavorable flow choking in the core of a trailing torus and increased heating to the base of the vehicle due to reverse flow [15,16]. In the case of the trailing sphere, impingement of the entry vehicle shock on the ballute produced levels of localized heating that were as high as twice those seen by the sphere alone. Heating results on the clamped ballute were the most favorable. Because the clamped ballute is attached directly to the base of the CEV, the boundary layer fully envelops both the ballute and the spacecraft. This has the effect of greatly increasing the effective nose radius of the CEV, thereby reducing convective heating significantly. Given that convective heating to the ballute is more likely to be a limiting factor than heating to the CEV, a further advantage of the clamped configuration is that the entry vehicle is exposed to a relatively benign aerothermodynamic environment. Lastly, although a clamped ballute will be 2–3 times more massive than a trailing ballute of an equivalent diameter, the reduction in heat rate provided by the clamped ballute allows for an overall smaller diameter and, thus, reduced system mass.

In summary, although the trailing sphere is favorable for its approximate mass-to-drag contribution ratio (β_b), the heating advantages provided by the clamped configuration are more applicable to the mission scenarios being studied. In view of this, the analysis henceforth will focus on using a clamped torus ballute. It should be mentioned that the preceding analysis focuses on only a few critical design parameters. A higher-fidelity analysis should include considerations of aeroelastic stability, drag distribution, and the ballute attachment method. For example, clamped ballutes may require additional structural stabilization parameters or increased inflation pressures which would contradict the basic approximation of equating ballute surface area to system mass.

B. Aerodynamics

As mentioned previously, the lunar-return entry vehicle analyzed is a scaled-up version of the Apollo command module. Because of the extensive amount of testing already done on this shape, aerodynamic data are readily available. Thus, the aerodynamic properties used for the entry vehicle were taken from published data [17].

For many of the ballute diameters evaluated, a sizeable portion of the entry trajectory is characterized with Knudsen numbers on the order of unity, indicating that transitional regime aerodynamics are

Table 1 Ballute performance characteristics for a torus ratio (R_t'/R_t) of five and CEV dimensions

Ballute type	Hypersonic C_D	β_b
Trailing torus	0.741	7.9
Trailing sphere	1.0	4.0
Clamped torus	1.496	5.9

important. To attain transitional values, the free-molecular and continuum aerodynamics were first estimated and then a bridging function was used. The free-molecular drag coefficients were calculated assuming a diffuse Maxwellian reflection model [18], where the values of the normal and tangential momentum accommodation coefficients σ_N and σ_T, respectively, are assumed equal to one. Calculation of the free-molecular pressure and shear forces was done using the following relations [18]:

$$\frac{\Delta p}{q_\infty}s^2 = \left[\frac{(2-\sigma_N)}{\sqrt{\pi}}s\sin\theta + \frac{\sigma_N}{2}\left(\frac{T_w}{T_\infty}\right)^{\frac{1}{2}}\right]\exp(-s^2\sin^2\theta) + \left[(2-\sigma_N)\left(\frac{1}{2}+s^2\sin^2\theta\right) + \frac{\sigma_N}{2}\left(\frac{T_w}{T_\infty}\right)^{\frac{1}{2}}\sqrt{\pi}s\sin\theta\right] \times [1+\mathrm{erf}(s\sin\theta)] \tag{3}$$

$$\frac{\Delta\tau}{q_\infty}s^2 = \frac{\sigma_N s\cos\theta}{\sqrt{\pi}}\{\exp(-s^2\sin^2\theta) + \sqrt{\pi}s\sin\theta[1+\mathrm{erf}(s\sin\theta)]\} \tag{4}$$

The molecular speed ratio s is comparable to the Mach number and can be calculated as follows:

$$s = \frac{V_\infty}{\sqrt{2RT_\infty}} \tag{5}$$

Equations (3) and (4) were numerically integrated over the surface of the ballute to attain the free-molecular aerodynamic coefficients.

Continuum regime drag coefficients were estimated from Newtonian impact theory. Under this method, the tangential or shear forces are neglected, and a simple relation for the pressure coefficient on an elemental area inclined to the freestream at an angle θ can be derived as

$$C_P \equiv \frac{\Delta p}{q_\infty} = 2\sin^2\theta \tag{6}$$

As opposed to the free-molecular pressure and shear coefficients, the Newtonian relation allows for an explicit integration over the surface of the ballute. As such, the zero angle-of-attack drag coefficient for a clamped torus ballute can be calculated from the following:

$$\mathrm{C}_{D,\mathrm{ballute}} = \left(\frac{R_n}{R_b}\right)^2[1-\sin^4\theta_b] + 2\sin^2\theta_b\left[\frac{(R_t'+R_t\cos\theta_b)^2}{R_b^2} - \left(\frac{R_n}{R_b}\right)^2\cos^2\theta_b\right] + \frac{4R_t(R_b-R_t)}{3R_b^2}[2-3\cos\theta_b+\cos^3\theta_b] + \left(\frac{R_t}{R_b}\right)^2\sin^4\theta_b \tag{7}$$

The reference area used to nondimensionalize Eq. (7) is based upon the ballute radius R_b. Additionally, Eq. (7) can be broken down by the contribution of each of the three main geometric elements of the clamped torus ballute. The first term in Eq. (7) is the drag coefficient of the spherical nose portion (the CEV forebody), the second term is the drag of the ballute conical frustum, and the last terms comprise the drag from the exposed portion of the ballute torus itself. For a given set of entry vehicle dimensions, the ballute half-cone angle θ_b can be calculated by assuming a smooth interface between the ballute and the entry vehicle heat shield yielding the following:

$$\theta_b = \cos^{-1}\left(\frac{D_c}{2R_n}\right) \tag{8}$$

Using the entry vehicle dimensions mentioned previously, a ballute cone angle of roughly 65 deg is calculated and is used for this study.

Determination of the transitional regime drag coefficients was done using the bridging function of Gorenbukh [18] provided as follows:

$$\frac{\mathrm{C}_D - \mathrm{C}_{D,\mathrm{cont}}}{\mathrm{C}_{D,\mathrm{FM}} - \mathrm{C}_{D,\mathrm{cont}}} = \frac{1}{\sqrt{2\pi}}\int_{-\infty}^{\log_{10}(Kn)+1.1403}\exp\left(-\frac{y^2}{2}\right)\mathrm{d}y \tag{9}$$

C. Trajectory

The analysis of atmospheric entry at Earth was done using the 3 degree-of-freedom version of the Program to Optimize Simulated Trajectories (POST) [19] assuming a standard 1976 atm. Atmospheric interface was assumed to occur at an altitude of 125 km. For lunar-return scenarios, entry velocities were kept constant at an inertial value of 11.1 km/s and entry flight-path angles were varied to within one-twentieth of 1 deg over a 5 deg corridor so as to closely evaluate skipout boundaries for each diameter. It is of interest to note that many of the more favorable ballute entry trajectories are near the limits of skipout and spend a significant amount of time in the upper atmosphere. Cargo-return scenarios assumed a fixed entry condition corresponding to a 100 m/s deorbit burn performed from the circular, 360 km altitude ISS orbit.

For this study, multiple entry trajectory strategies were investigated. In all cases, the ballute was assumed deployed in-space before reaching atmospheric interface. The first strategy consisted of using the ballute through the entire entry. An alternative strategy is to simply jettison the ballute after some predetermined velocity decrement. The jettison concept represents a hybrid aerocapture/direct-entry approach that attempts to use the ballute to dissipate energy until the lunar entry becomes similar to entry from low Earth orbit. In this strategy, the trajectory segment that made use of the ballute was flown with a zero angle-of-attack. Subsequent to ballute jettison, ballistic and lifting ($L/D = 0.3$) CEV trajectory options were investigated. An L/D of 0.3 is based upon that provided by the Apollo capsule at its trimmed angle-of-attack and planned for the CEV.

Although guidance was neglected for this level of study, a more detailed analysis would need to account for many of the intricacies involved in using large inflatable drag devices. For example, large ballutes can reach relatively low velocities very high in the atmosphere, thus increasing their susceptibility to wind variations and enlarging the landing footprint. Typical guidance strategies for ballutes involve either some form of drag modulation through reefing or staged deployment, or utilization of lift through nonaxisymmetric ballute shapes. Though they introduce interesting opportunities for trajectory refinement, both of these strategies are beyond the scope of this work.

D. Aeroheating

Estimations of the aeroheating encountered by the ballute and entry vehicle were done using two stagnation-point heating approximation methods. Convective heating was calculated using the correlation provided by Sutton and Graves [20]. During Earth entry at lunar-return velocities, radiative heating from the shock layer contributes considerably and must not neglected. Toward this end, the method for estimating radiative heat rates by Tauber and Sutton [21] is used. A major variable in both formulations is the effective nose radii. For large clamped ballutes this nose radius is much greater than that of the entry vehicle alone. Examination of computational fluid dynamics (CFD) cases completed as part of the aerocapture technology portion of NASA's In-Space Propulsion Program [22] indicated that the effective nose radius of a clamped ballute as a percentage of the ballute diameter increases as the ballute diameter increases. Based on this CFD analysis, an approximation was used in this investigation to estimate the effective nose radius as linearly varying between one-quarter of the diameter for a 25 m ballute and three-quarters of the diameter of a 100 m ballute. The effective nose radius for ballutes larger than 100 m was kept constant at three-quarters diameter. Although larger effective nose radii significantly reduce convective heating, they also increase radiative heating [23]. Thus, depending on the proportion of peak heating due to radiative effects, larger ballute diameters can incur higher heating rates than smaller ones. Though this general behavior is captured by the two conceptual design heating methods employed, more detailed

analysis will be required to validate the calculated levels of heating, particularly the radiative portion.

E. Mass Estimation

The total ballute entry system was considered as four components consisting of the ballute material, the pressurant required to inflate the ballute, the pressurant tankage, and a fixed mass associated with pressure transducers, valves, fittings, and other mechanical/electrical systems. Ballute mass was calculated from the total surface area of the ballute for a given average areal density of ballute material. Pressurant mass was calculated as a function of the internal volume of the ballute using nitrogen gas. The amount of nitrogen required was determined by assuming a required ballute inflation pressure of twice the peak dynamic pressure, with an additional 15% margin. No accommodation was made in this mass estimation for pressurant gas leakage due to ballute seam porosity. With the amount of required nitrogen known, tankage mass was estimated using the following relationship [24]:

$$m_{\text{tank}} = \frac{m_{N_2} R_{N_2} T_{\text{tank}}}{g_0 \phi_{\text{tank}}} \tag{10}$$

For the tank-mass factor ϕ_{tank} a value of 6350 m corresponding to a typical titanium pressurant tank was used.

III. Results and Discussion

A. Performance Analysis

1. Lunar-Return Missions

The first portion of this investigation focused on evaluating the trajectory and heating characteristics of a ballute entry for a 9500 kg CEV on lunar return. The evaluation included both a characterization of the entry design space and an examination of multiple ballute entry strategies. CEV assumptions, entry mass, and ballute half-cone angle were kept constant and the ballute diameter was varied (from 30 to 200 m). The primary metrics of interest were peak heat rate, peak deceleration, and peak dynamic pressure. The first of these is provided in Fig. 4, along with a shaded region corresponding to overshoot conditions. The overshoot boundary is defined as the point at which the vehicle will no longer reach the surface and instead depart the Earth's atmosphere and enter Earth orbit. At lower ballute diameters, modest increases in ballute diameter exhibit large decreases in peak heat rate due to both deceleration at higher altitudes and to an increased effective nose radius. However, this trend quickly plateaus as the proportional change in ballistic coefficient becomes less and the effective nose radius increases to 75% of the ballute diameter. Although material heating limits are discussed in greater detail in a subsequent section, candidate thin-film materials (without the addition of TPS) typically have temperature limits less than 900 K, which, assuming radiative equilibrium conditions, corresponds to a heating limit of roughly 3.0 W/cm^2. Under these constraints, thin-film ballute diameters of at least 140 m would be required for Earth return of the CEV from the moon.

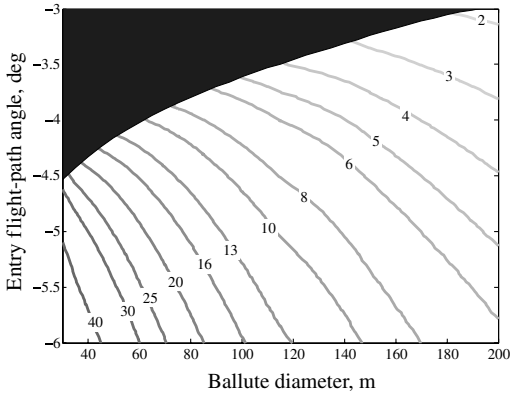

Fig. 4 Peak heat rate (W/cm^2) contours for an 11.1 km/s, 9.5 t entry without ballute jettison.

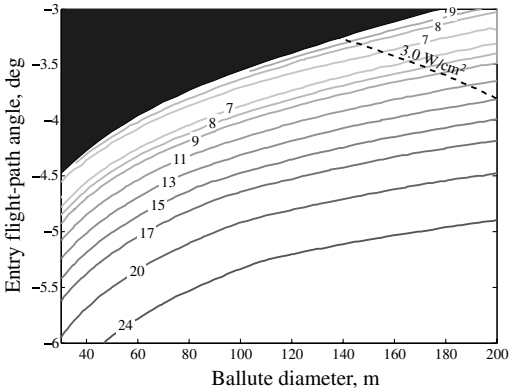

Fig. 5 Peak deceleration (g) contours for an 11.1 km/s, 9.5 t entry without ballute jettison.

The second metric of interest is primarily due to the inclusion of human passengers on this lunar-return vehicle. As shown in Fig. 5, for a given flight-path angle, the peak deceleration tends to decrease with decreasing ballute size. More interesting perhaps is that, unlike peak heat rate, for a fixed ballute size, the minimum value of peak deceleration does not occur at the overshoot condition but rather a few tenths of a degree away from this boundary. This indicates that entry trajectories that seek to minimize peak heat rate do so at the expense of increased deceleration loads. In the case of the 3.0 W/cm^2 heating constraint (shown overlaid in Fig. 5), this would either mean keeping the 140 m ballute and taking the penalty in g-loads (approximately 9 g) or moving to a larger ballute so as to be able to tolerate the increased heat rate of a slightly steeper entry. For the 3.0 W/cm^2 case, a ballute diameter of roughly 160 m minimizes peak deceleration. The analysis also gives insight into the width of the deceleration limited entry corridors. For example, restricting an entry to 7 g, the same as that encountered by the Apollo astronauts, implies a total entry flight-path angle corridor width of approximately 0.25 deg. Though narrow, this corridor width is well within recently demonstrated navigational capabilities [25].

Results for peak dynamic pressure are provided in Fig. 6. Occurring simultaneously with peak deceleration, peak dynamic pressure is of interest primarily for its impact on the design of the ballute. In particular, a lower peak dynamic pressure allows for lower inflation pressures, reduces material strength requirements, and reduces the likelihood of adverse structural dynamic response. Again limiting the ballute to a heat rate of 3.0 W/cm^2, it can be seen that dynamic pressures close to 25 Pa will be encountered. As was the case with the deceleration contours, the optimum dynamic pressure conditions do not occur at the overshoot boundary.

Altitude, velocity, and deceleration profiles are provided in Fig. 7 for a 100-m-diam ballute system over a range of entry flight-path

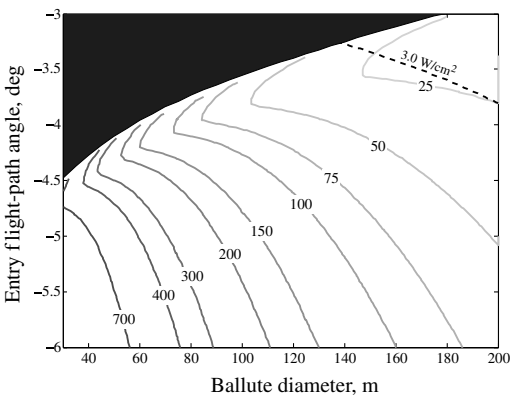

Fig. 6 Peak dynamic pressure (Pa) contours for an 11.1 km/s, 9.5 t entry without ballute jettison.

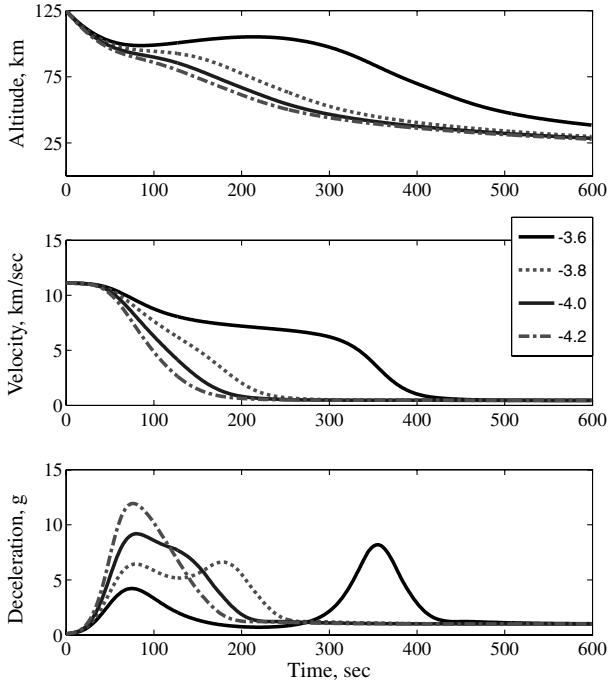

Fig. 7 Altitude, velocity, and sensed deceleration profiles for a 100-m-diam ballute over a range of entry flight-path angles.

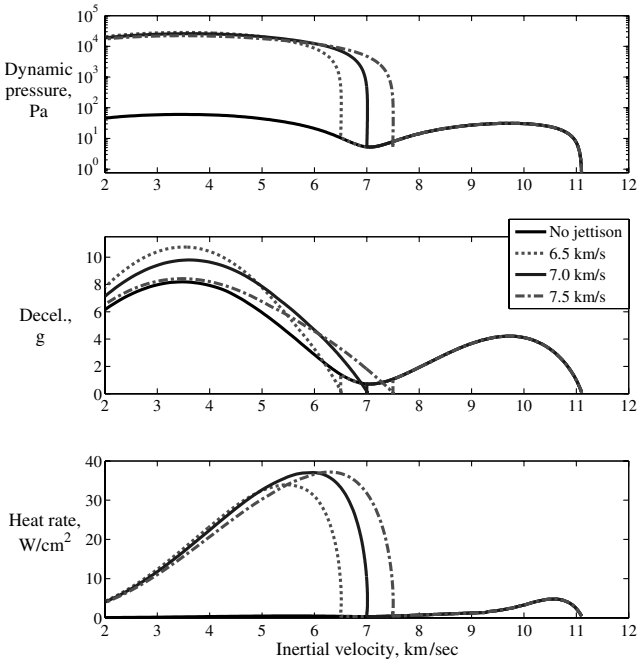

Fig. 8 Trajectory effects of varying jettison velocities on a near skipout entry of a 9.5 t vehicle using a 100 m ballute and entering at 11.1 km/s (postjettison entry is ballistic).

angles. Entry at flight-path angles just shy of the overshoot boundary (e.g., −3.6 deg) results in multiple skips. During the first portion of the entry, the ballute dissipates enough energy so as to remain on an eventual touchdown trajectory. The deceleration profile is multipulsed with the majority of the deceleration occurring during the second entry. As the entry flight-path angle steepens, more deceleration is achieved in the first pass and the magnitude of the second pulse lessens. The minimal peak deceleration occurs when the two pulses are roughly equivalent ($\gamma = -3.8$ deg with a peak deceleration of approximately 5 g for the example in Fig. 7). However, minimizing deceleration magnitude comes at the expense of an extended pulse duration. Further steepening of the entry merges the two pulses and the maximum deceleration value increases again.

For a 9500 kg CEV payload, the entry strategy of not jettisoning the ballute is shown to require a ballute diameter greater than 100 m, depending on the heating and dynamic pressure limits placed on the ballute. It should be noted that these hypersonic results apply whether the ballute is carried to the surface or discarded in the subsequent supersonic or subsonic flow conditions. Although previously proposed for landing large payloads on Mars [26], retention of the ballute through transonic and subsonic conditions would require significantly more knowledge in the behavior of inflatable structures than is encompassed in this study.

An alternative to retaining the ballute through the entire hypersonic entry is to deploy the ballute for a predetermined velocity decrement and then release the ballute. In a typical aerocapture strategy, the ballute is used to dissipate enough energy from the hyperbolic approach trajectory to transition to a closed Earth orbit in a single pass [27]. In this investigation, a hybrid entry strategy is proposed that enters at a slightly steeper flight-path angle so that, upon ballute release, the entry vehicle follows a modified Earth entry trajectory. Demonstration of this effect is provided in Fig. 8, in which different release velocities are plotted against a no-release trajectory for a 100-m-diam ballute entering at a −3.6 deg inertial flight-path angle. In this manner, the deceleration encountered by the ballute can be directly traded against that placed on the CEV. Releasing the ballute earlier increases the heating encountered by the CEV but mitigates the strength (driven by dynamic pressure) requirements of the ballute. For the trajectory shown in Fig. 8, ballute jettison occurs before the second, stronger dynamic pressure pulse, reducing the peak dynamic pressure encountered by the ballute. However, heating limitations on the ballute cannot be avoided, as peak heating occurs at velocities of about 10.5 km/s.

Two strategies for descent after ballute jettison were evaluated, one in which the vehicle continued on a ballistic trajectory, and the other in which the vehicle transitioned to a lifting trajectory with an L/D of 0.3. The former approach is favorable for its simplicity, whereas the latter approach may be necessary for targeting purposes. Beginning with the ballistic condition, entries with ballute jettison can be shown to provide several advantages. Shown in Fig. 9 are CEV heating contours over a range of inertial jettison velocities for the lunar-return case. Provided on the abscissa are the peak heating rates on the ballute before jettison. Examination of the peak heating rates (encountered by the CEV after ballute jettison) shows the potential to mitigate vehicle heat rates to less than 35 W/cm^2, or roughly the limit of an existing reusable thermal protection system. Also evident is that this capability exists over a range of ballute diameters with the primary constraint being the heating limitations on the ballute itself.

These lower heating rates are attained at two separate ranges of jettison velocities, a higher range that lets the CEV alone decelerate more at higher altitudes and a lower range that releases the entry vehicle in a thicker atmosphere at a lower velocity. Provided in Fig. 10 are peak deceleration contours over a range of jettison velocities. The peak deceleration values plotted correspond to the larger value of either the peak deceleration during the ballute segment of flight or the peak deceleration seen after ballute release. At the lower ballute heat rates (shallower entry angles), peak deceleration occurs after ballute jettison. At steeper entry angles, the ballute deceleration pulses are merged (see Fig. 7) and the peak deceleration occurs before ballute release. Although favorable heating conditions can occur at both low and high jettison velocities, deceleration considerations (see Fig. 10) favor high jettison velocities as they eliminate the second, larger ballute deceleration pulse. Figure 11 shows the peak dynamic pressure condition during the ballute segment of flight. In contrast to retaining the ballute, jettison can reduce the maximum dynamic pressures by as much as 50%, particularly for entry conditions near skipout. Whereas achieving the lowest dynamic pressures without ballute jettison required entering at a flight-path angle associated with a higher heat rate (see Fig. 6), the ballute jettison strategy is able to collocate minimum heating and minimum dynamic pressure at the overshoot

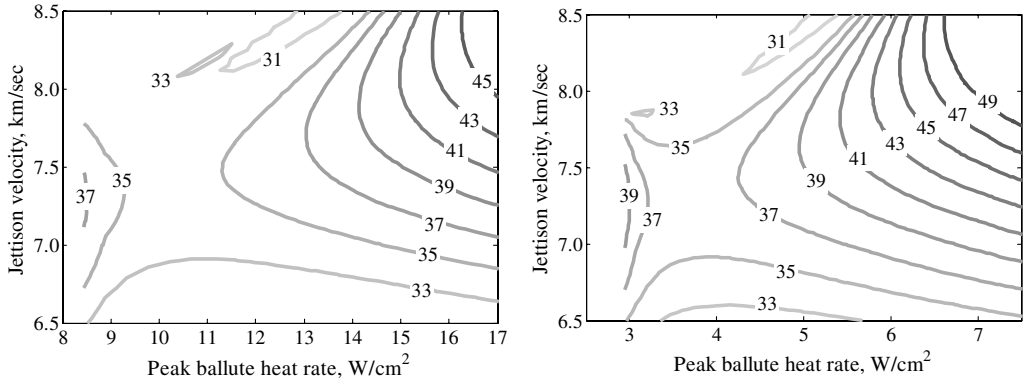

Fig. 9 Peak CEV heat rate (W/cm^2) contours with lifting entry after jettison for ballute diameters of a) 70 m and b) 140 m for an 11.1 km/s entry.

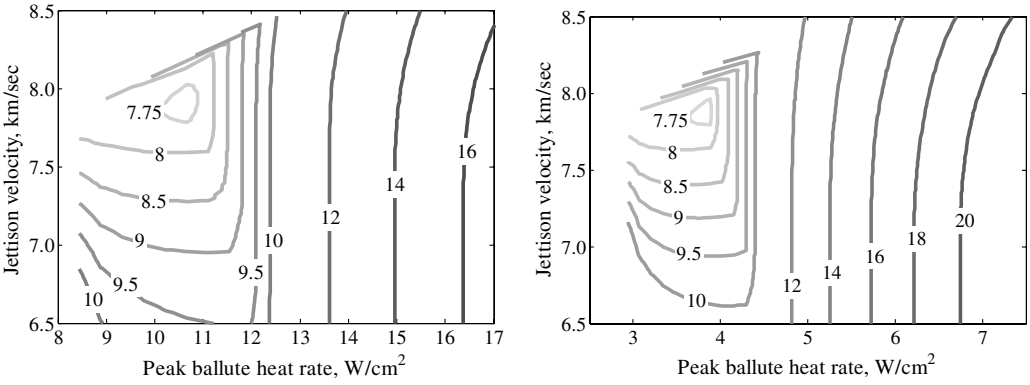

Fig. 10 Peak deceleration contours (g) with lifting CEV entry after jettison of a) 70 m and b) 140 m ballutes for an 11.1 km/s entry.

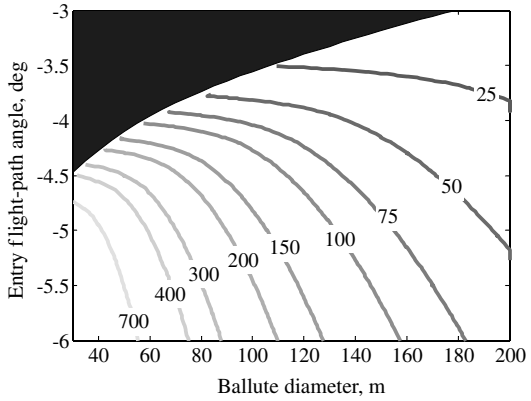

Fig. 11 Peak dynamic pressures (Pa) encountered by ballute before jettison for a 9.5 t, 11.1 km/s entry.

boundary. Though not shown, variation of the velocity at which the ballute was released has little or no impact on peak dynamic pressure.

Entry vehicle heating contours for a lifting postballute entry are shown in Fig. 12. Compared with the ballistic entry, using a moderate degree of lift ($L/D = 0.3$) reduces the CEV heat rates to well within reusable limits for nearly all of the entry angles and jettison velocities evaluated. Again, this trend holds over a range of ballute diameters, once more indicating that the thermal limitations of the ballute material (as indicated by the abscissa in Figs. 9 and 10) will drive ballute feasibility more than the requirement for a certain velocity decrement. That is to say, 70 m ballutes can be used to significantly reduce CEV heating just as well as 140 m ballutes, so long as the ballutes themselves are capable of handling the increased heating. Improvement in peak deceleration, shown in Fig. 13, is also evident when lift is introduced. At the shallowest entries, maximum deceleration can be reduced to 4–4.5 g, depending on the ballute size. Additionally, the peak deceleration is shown to be almost completely independent of the jettison velocity.

In addition to the 9500 kg crewed lunar CEV, investigation into lower mass lunar cargo vehicles, using the same basic dimensions as the CEV, were performed. As it is not expected that cargo variants will have as strict a requirement on deceleration loads as a crewed vehicle, ballute entries that retain the ballute through supersonic flight conditions were investigated.

Minimum peak heat rate results for this portion of the study are provided in Fig. 14. These heat rates correspond to entry at flight-path angles at the overshoot boundary and thus correspond to the minimum heat rate possible for a given entry mass and ballute size. Again using a 3.0 W/cm^2 heat rate limitation, it can be seen that a reduction in CEV entry mass of 1000 kg allows for a roughly 10 m reduction in required ballute diameter. The 100:1 ratio provides an excellent rule of thumb for future lunar entry design considerations.

Contours of peak dynamic pressure and overshoot boundaries are provided in Figs. 15 and 16, respectively. The plotted dynamic pressure values correspond to entry flight-path angles yielding the lowest peak dynamic pressure and not to the overshoot boundaries.

2. *Low-Earth-Orbit Return Missions*

The investigation into using a ballute for LEO cargo-return missions sought to characterize the ability of a ballute to mitigate entry loads, particularly in the realm of heating. However, rather than acting as an enabler for the use of an already existing TPS solution, the focus here is to use ballutes in lieu of a more traditional TPS system altogether. That is, to evaluate the feasibility of using a ballute system to provide entry capability where none previously existed. In

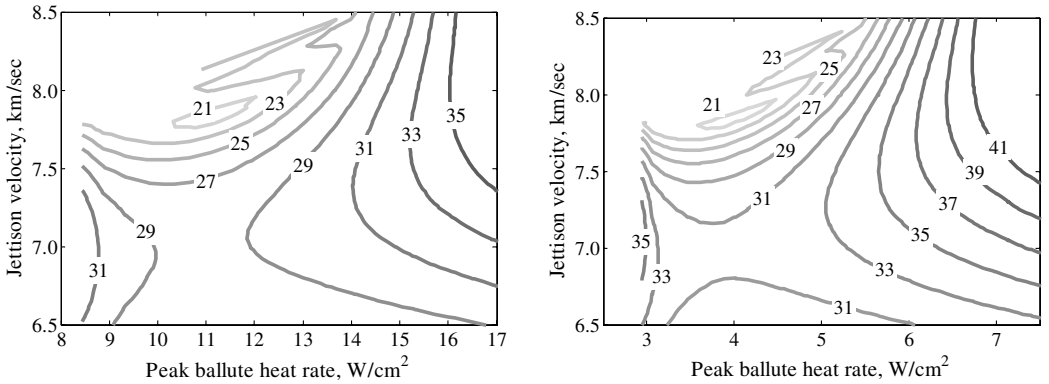

Fig. 12 Peak CEV heat rate (W/cm^2) contours with lifting entry after jettison for ballute diameters of a) 70 m and b) 140 m for an 11.1 km/s entry.

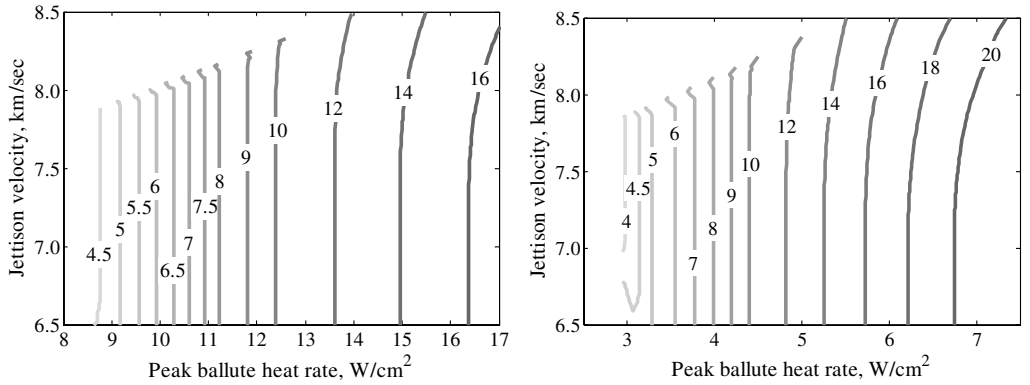

Fig. 13 Peak deceleration contours (*g*) for ballistic CEV entry after jettison for ballute diameters of a) 70 m and b) 140 m for an 11.1 km/s entry.

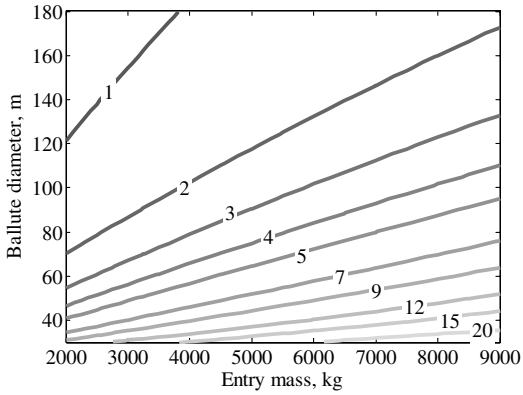

Fig. 14 Peak heating (W/cm^2) contours at the overshoot boundary of an 11.1 km/s entry.

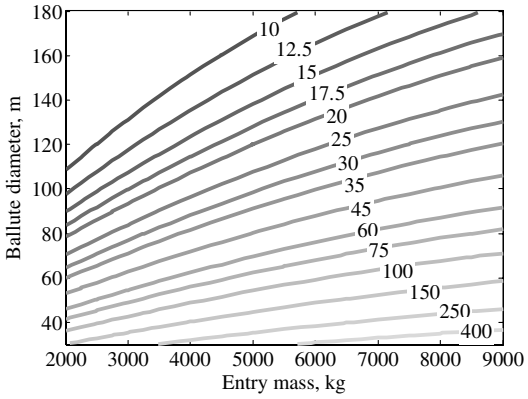

Fig. 15 Minimum peak dynamic pressures (Pa) for an 11.1 km/s entry over a range of entry masses and ballute diameters.

contrast to lunar-return entry, entry from a given low Earth orbit is less sensitive to minor variations in flight-path angle, and thus entry parameters were kept fixed at an inertial velocity of 7870 m/s and a flight-path angle of −1.4 deg. These conditions correspond to performing a 100 m/s deorbit burn from ISS orbit and lowering perigee to an altitude of about 21 km. Although skipping entries were previously shown to be favorable for lunar-return purposes, they are here eschewed, as they increase the complexity of targeting a specific landing site when an active guidance system is not employed. Entry mass was varied from 1 to 20 t, with the upper limit corresponding to a fully loaded automated transfer vehicle. The range of ballute diameters considered varied from 10 to 150 m.

As mentioned, primary emphasis was on heat rate impacts, and these are provided in Fig. 17. It is immediately recognized that even small diameter ballutes can provide a reasonably low peak heat rate. At the higher entry masses, ballute diameters of no more than roughly 48 m are required to bring peak heating to within 3.0 W/cm^2. Additionally, given that even relatively small ballutes in the range of 15 m diameter can reduce heating to within 15 W/cm^2, the potential exists to move beyond thin-film ballute concepts and instead rely on thicker, and more massive, multilayered insulation material stacks designed to withstand higher heat rates. Lastly, although only the thermal limitations of the ballute material are considered, temperature limits on the structure of a

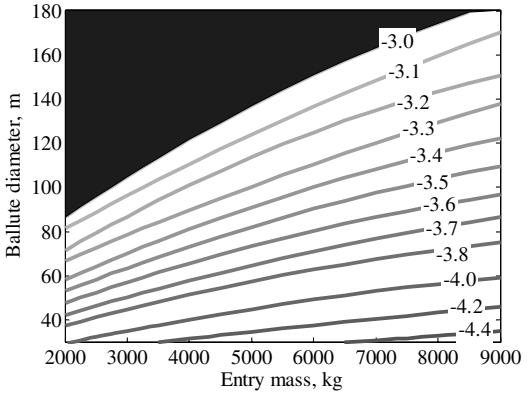

Fig. 16 Overshoot entry flight-path angle boundaries for an 11.1 km/s entry over a range of entry masses and ballute diameters.

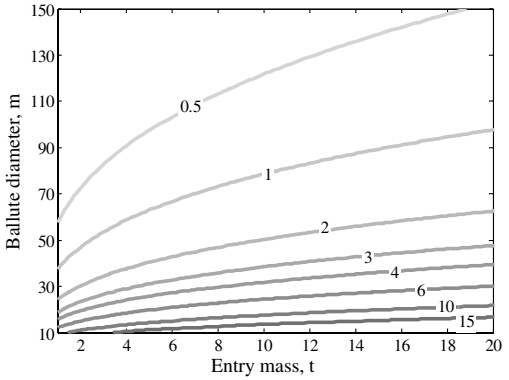

Fig. 17 Peak heating (W/cm^2) contours for ballute entry from low Earth orbit.

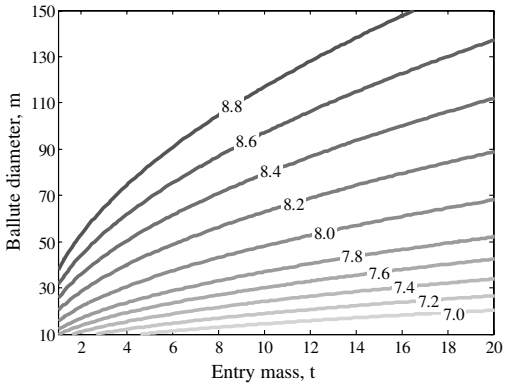

Fig. 18 Peak deceleration magnitude (g) for ballute entry from low Earth orbit.

converted transfer vehicle may require additional insulation, e.g., thermal blankets.

Examining the other two metrics of interest, deceleration magnitude and dynamic pressure, provides a similarly favorable result. Provided in Figs. 18 and 19 are plots of the peak deceleration magnitude and peak dynamic pressure, respectively. For the assumed entry flight-path angle, peak deceleration values are kept to less than 9 g, and as low as 7 g, across the full range of configurations studied. It should be mentioned that, although contours are not shown, the upper left portion of Fig. 18 corresponds to a relatively constant value of 8.8 g. Although these values may be considered too high for certain biological experiments, they should be suitable for inanimate cargo. As before, regions of favorable heating are seen to be in conflict with favorable peak deceleration pulses, indicating that peak deceleration is likely to be greater than 8 g, due to thermal restrictions (assuming a 3.0 W/cm^2 constraint).

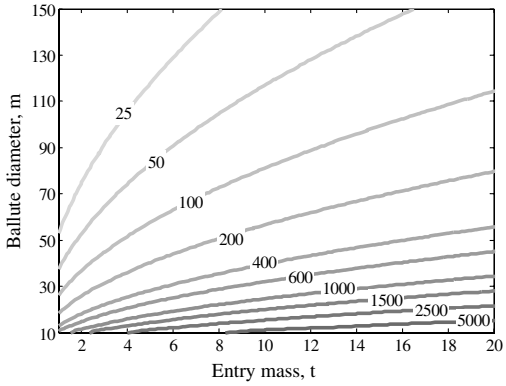

Fig. 19 Peak dynamic pressure (Pa) for ballute entry from low Earth orbit.

For structural considerations, peak dynamic pressures encountered by the ballute are likely no higher than about 1000 Pa.

B. Sizing and Mass Evaluation

From the mass model introduced earlier, several sizing trends are evident. Provided in Fig. 20 are contours of ballute systems mass for different sized ballutes and material densities. At larger diameters, attaining a ballute system mass on the order of several metric tons requires an average material density of 0.15 kg/m^2 or less. Note that the slope of the contours provides insight into the relative importance of the material areal density on the total system mass. In particular, for a constant ballute diameter, doubling the areal density nearly doubles the ballute system mass. Indeed, for a fill pressure of 100 Pa, the mass of the ballute material alone represents almost 85% of the total ballute system mass at even the lowest areal densities. Though not shown, doubling or halving the fill pressure changes the relative contribution to about 75 and 90%, respectively.

Given its importance in determining the overall mass of a ballute system, achieving low material mass is a primary technical hurdle toward ballute feasibility. Achieving low areal densities is complicated by the thermal and strength limitations of many candidate materials. Previous conceptual studies [1,10,27] have focused on using thin-film materials such as Kapton and Polyboxoxazole, which have operational temperature limits between 500 and 600°C [1,10] and areal densities of about 0.075 kg/m^2. The low temperature limits of thin films have led to a focus on using various types of multilayer insulation (MLI). These concepts typically consist of one of the aforementioned polymer films as an internal bladder combined with additional layers of adhesives, metal foils, and outer layer fabrics (such as Nextel) that are designed to resist much higher heating conditions. One such concept [28] was tested at heat rates as high as 35 W/cm^2 without observable damage. Although this concept had a sizeable average areal density of about 1.86 kg/m^2, its thermal characteristics make it favorable for regions of a ballute seeing the most heating. The IRVE flight demonstrator

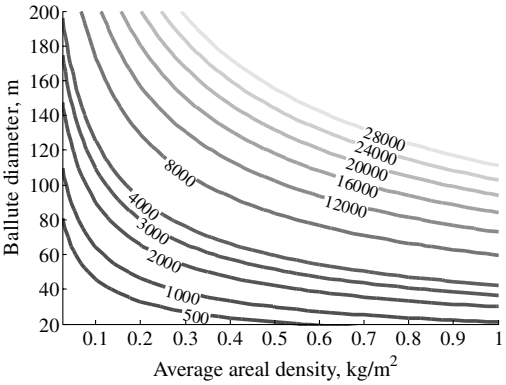

Fig. 20 Ballute system mass (kg) at an inflation pressure of 100 Pa.

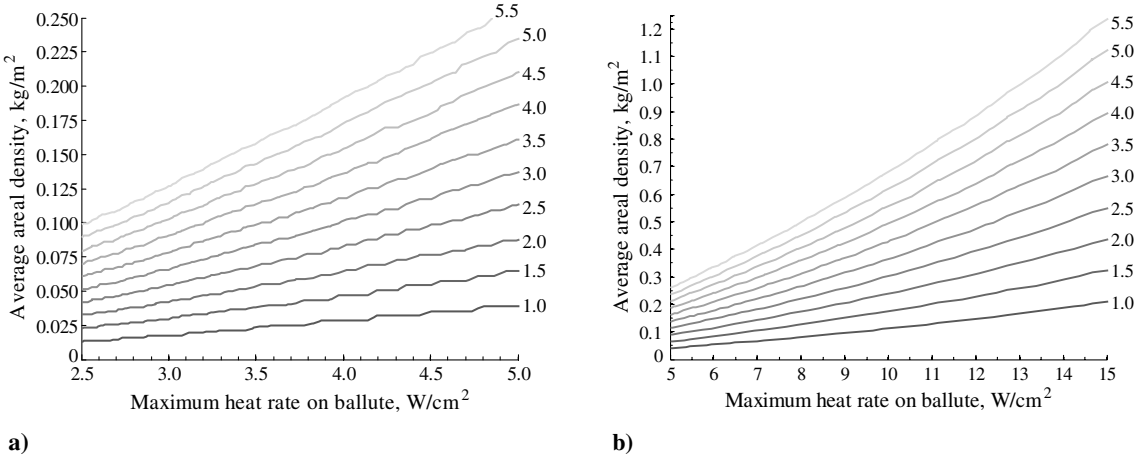

Fig. 21 Ballute entry system mass (t) as a function of maximum ballute heat rate and average areal density for an entry mass of 9.5 t and an entry velocity of 11.1 km/s.

[4] that launched in 2007 has baselined a ballute that incorporates a silicone coated Kevlar fabric for the bladder to mitigate tear risk. The remainder of the material stack consists of a dry Kevlar restraint ply, a Kapton gas barrier, and several layers of Nextel cloth for thermal protection. Material thickness for the IRVE concept varies along the radius of the ballute, however, the entire demonstrator incorporating a 3 m ballute is less than 100 kg.

From the 9500 kg lunar CEV trajectory results that incorporated ballute jettison, one can estimate a required ballute diameter as a function of a limiting heat rate on the ballute. The calculated diameter can then be used to evaluate a required average material density for a specific ballute system mass. Results from this analysis are provided in Fig. 21. Assuming an entirely thin-film ballute with its corresponding areal density (0.075 kg/m^2) and a 900 K temperature limit yields a ballute system mass of about 3.5 t, or nearly 37% of the assumed CEV mass. For comparison, the thermal protection system for the Apollo command module constituted slightly less than 30% of the capsules gross mass [6]. Achieving a similar mass fraction for the ballute alone would correspond to a system mass of 2.85 t, which would require significant improvements in either areal density or temperature limits of the material concepts previously mentioned. The most direct means of improvement in the mass estimates computed in this investigation are improvements in material areal density and thermal limitations. For example, assuming the same 3.0 W/cm^2 limit as before, a ballute with an areal density of 0.025 kg/m^2 would allow for mass fractions of around 13%.

The same methodology of equating ballute diameter to a given heat rate constraint and backing out a required areal density was applied to the cargo CEV variants. These results, as a percentage of the entry mass, are provided in Fig. 22. The lines of ballute system mass fraction shown in Fig. 22 represent quadratic least-squares regression fits to the full range of entry masses. Of interest is that the plotted trends are observed to hold quite well regardless of entry mass. In other words, for the lunar-return case, and for a given heat rate limitation and ballute areal density, the ballute system mass is roughly a fixed percentage of the entry mass. The fixed mass percentage result further underscores the importance of material properties on ballute system design. That is, if viability is measured by the ballute system mass fraction, then a direct correlation between viability and the material properties of the ballute is evident.

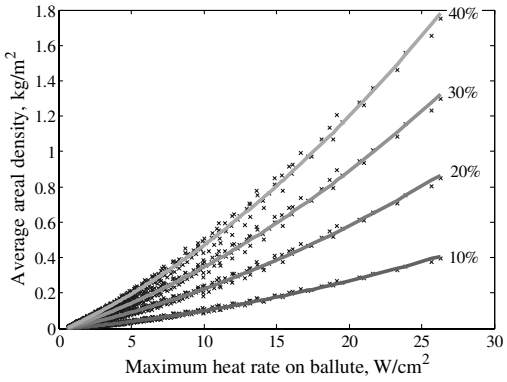

Fig. 22 Ballute entry system mass percentages as a function of heat rate limitations and average areal density for an entry velocity of 11.1 km/s.

Provided in Fig. 23 are areal density curves for the LEO return cases. The broader range of entry masses examined prevented a simple least-squares regression from accurately portraying all cases, and thus curves are provided for three distinct entry masses. Examination of these trends provides further evidence toward the feasibility of using ballutes for ISS downmass missions. In the low range of entry masses, Fig. 23a, a thin-film ballute has a mass fraction of less than 10% of the total entry mass. Heavier masses (corresponding to a fully loaded ATV or HTV) could instead use thicker MLI stacks designed specifically for higher heating loads, such as the aforementioned 1.86 kg/m^2 concept, and achieve even lower mass fractions. Although the ballute mass fractions are promising, it is likely that additional mass in the form of a terminal descent system may be required. The combined entry system mass would also reduce the upmass capability of the resupply vehicles.

IV. Conclusions

This paper focused on analyzing the potential benefits that a clamped ballute entry system can provide to near-term human- and cargo-return missions from the moon and the ISS. Lunar-return missions were evaluated assuming a capsule-shaped entry vehicle with a nominal mass of 9500 kg entering Earth's atmosphere at 11.1 km/s. For trajectories that retained the ballute through hypersonic flight, heat rates were observed to vary from 40 W/cm^2 for a 40-m-diam ballute to as low as 2 W/cm^2 for a 200-m-diam ballute. Peak deceleration values as low as 6 g were possible, but generally exceeded 7 g. For larger ballutes, in excess of 100 m, dynamic pressures of about 75 Pa were experienced. Minimum deceleration and dynamic pressure both occurred at flight-path angles slightly steeper than the overshoot boundary. This phenomenon occurred due to the skipping nature of shallow entries, producing multiple deceleration pulses with the latter one being the strongest. Ballute system performance was improved by jettisoning the ballute after a significant velocity decrement. For entries that maintained ballistic flight after ballute jettison, entry vehicle heat rates calculated were within reusable TPS limits of 35 W/cm^2. However, peak deceleration values generally exceeded 7.75 g. Minimization of heat rate, peak deceleration, and dynamic pressure favored ballute jettison at an inertial velocity of around 7.8 km/s. Entries that transitioned to an L/D of 0.3 after ballute release provided further mitigation of heating and deceleration on the CEV.

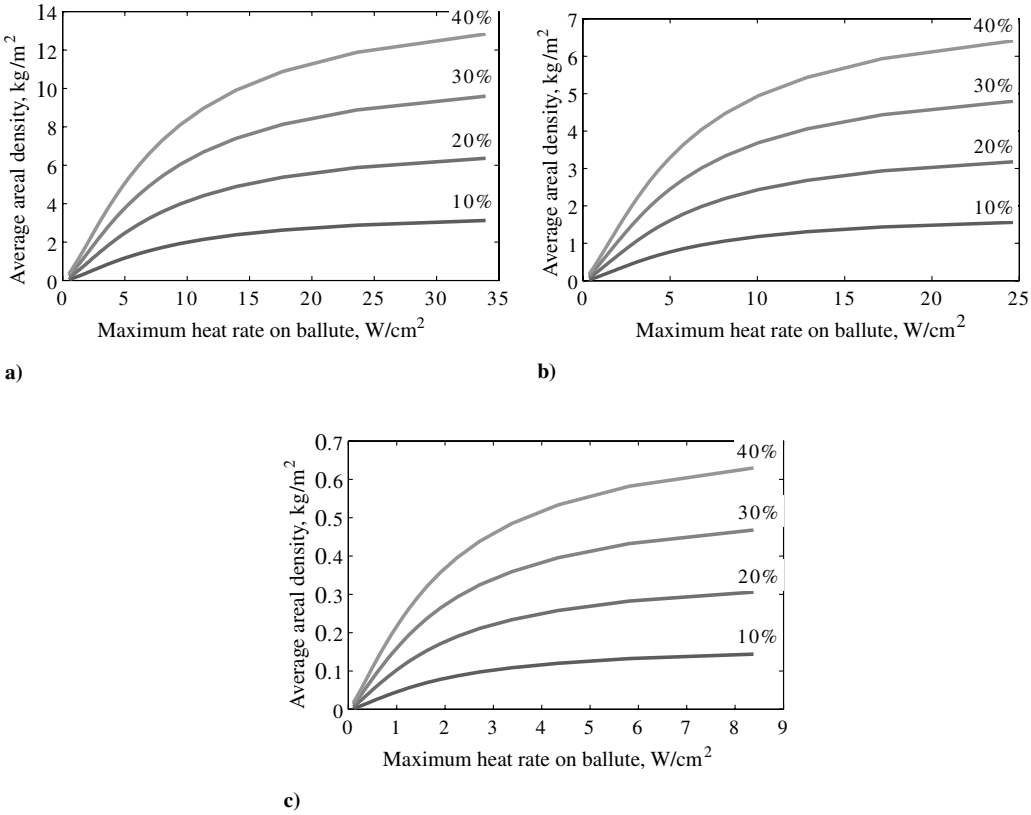

Fig. 23 Ballute entry system mass fraction for cargo return from low Earth orbit for entry masses of a) 1 t, b) 10 t, and c) 20 t.

Heat rates as low as 21 W/cm^2 and decelerations as low as 4 *g* were possible. Reductions in heating and deceleration were achieved over a range of ballute diameters, indicating that ballute sizing is primarily driven by the heating constraints of the ballute material. Variations in entry mass for a lunar-return cargo variant of the CEV were also investigated. For a heat rate limitation of 3.0 W/cm^2, each metric ton reduction in entry vehicle mass allowed for a 10 m reduction in required ballute diameter.

Examination of ballute entry from low Earth orbit showed the potential for using ballutes on ISS resupply vehicles. A fully loaded ATV or HTV resupply vehicle requires a ballute diameter of 48 m to meet thin-film thermal limitations. Replacing thin films with higher density MLI materials, which have more favorable thermal limitations, allows for ballute system mass fractions of approximately 7%.

Ballute systems were sized to evaluate mass requirements. Trends of required average areal density of the ballute vs heat rate limitations for a given ballute system mass were generated. These contours provide guidance as to the technical requirements that a candidate ballute must meet. Mass estimates assuming a thin-film material produced vehicle mass fractions of 37% for the 140 m ballute system. Reducing the areal density by two-thirds subsequently reduced the mass fraction to less than 13%, demonstrating the high sensitivity of ballute mass fraction to areal density. For lunar-return cases, varying entry mass was observed to have little impact on the ballute mass fraction for a given design concept (areal density and heating constraint). Material requirements exceeding 30% mass fraction indicate that continued technology development is likely required for lunar-return concept viability. However, applying current ballute technology toward ISS downmass missions appears promising. In particular, thick MLI ballute concepts can yield 15-m-diam systems that contribute less than 10% toward the total entry mass.

Acknowledgments

This work was completed as part of a larger study entitled "Ultralightweight Inflatable Thin-Film Ballutes for Human Return from the Moon," performed for the NASA Exploration Systems Human and Robotic Technology program through NASA Broad Area Announcement 04-02. The authors wish to thank James Masciarelli of the Ball Aerospace and Technology Corporation for leading this NASA-contracted study and for valuable insight regarding the technical scope of this systems analysis effort.

References

[1] Miller, L. K., Gulick, D., Lewis, J., Trochman, B., Stein, J., Lyons, D. T., and Wilmoth, R. G., "Trailing Ballute Aerocapture: Concept and Feasibility Assessment," AIAA Paper 2003-4655, July 2003.

[2] Westhelle, C. H., and Masciarelli, J. P., "Assessment of Aerocapture Flight at Titan Using a Drag-Only Device," AIAA Paper 2003-5389, 2003.

[3] Graesslin, M., and Schoettle, U., "Flight Performance Evaluation of the Re-Entry Mission IRDT-1," International Astronautical Federation Paper 01-V.3.05, Oct. 2001.

[4] Hughes, S. J., Dillman, R. A., Starr, B. R., Stephan, R. A., Lindell, M. C., Player, C. J., and Cheatwood, F. M., "Inflatable Re-entry Vehicle Experiment (IRVE) Design Overview," AIAA Paper 2005-1636, May 2005.

[5] Rohrschneider, R. R., and Braun, R. D., "Survey of Ballute Technology for Aerocapture," *Journal of Spacecraft and Rockets*, Vol. 44, No. 1, Jan.–Feb. 2007, pp. 10–23. doi:10.2514/1.19288

[6] Anon., "Apollo Program Summary Report: Synopsis of the Apollo Program Activities and Technology for Lunar Exploration," NASA TM-X-68725, April 1975.

[7] Moore, D. C. L., and Peri, F., "Exploration Technology Development Program," AIAA Paper 2007-136, Jan. 2007.

[8] Tran, H. K., Johnson, C. E., Rasky, D. J., Hui, F. C. L., Hsu, M., and Chen, Y. K., "Phenolic Impregnated Carbon Ablators (PICA) for Discovery Class Missions," AIAA Paper 96-1911, June 1996.

[9] Rasky, D. J., Harper, L., Newfield, M., and Smith, C., "Opportunities and Challenges for Supporting Commercial Space at NASA," AIAA Paper 2007-6154, Sept. 2007.

[10] Masciarelli, J. P., Lin, J. K. H., Ware, J. S., Rohrschneider, R. R., Braun, R. D., Bartels, R. E., Moses, R. W., and Hall, J. L., "Ultra Lightweight Ballute for Return to Earth from the Moon," AIAA Paper 2006-1698, May 2006.

[11] Anon.,"NASA's Exploration Systems Architecture Study," NASA TM-2005-214062, Nov. 2005.
[12] Bartels, R. E., Moses, R. W., Scott, R. C., Templeton, J. D., Cheatwood, F. M., Gnoffo, P. A., and Buck, G. M., "Proposed Role of Aeroelasticity in NASA's New Exploration Vision," *International Forum on Aeroelasticity and Structural Dynamics*, Deutsche Gesellschaft fr Luft- und Raumfarht Paper IF-013, 2005.
[13] Rohrschneider, R., "Variable-Fidelity Hypersonic Aeroelastic Analysis of Thin-Film Ballutes for Aerocapture," Ph.D. Thesis, Georgia Inst. of Technology, Atlanta, GA, May 2007.
[14] Foster, M. A., and Sirko, R. J., "Leveraging Existing Space Assets for Delivery of Cargo to the International Space Station," AIAA Paper 2006-7267, Sept. 2006.
[15] Gnoffo, P. A., and Anderson, B. P., "Computational Analysis of Towed Ballute Interactions," AIAA Paper 2002-2997, June 2002.
[16] Anderson, B. P., "Computational Continuum and Rarefied Flow Results for Ballute Applications," AIAA Paper 2004-292, Jan. 2004.
[17] Graves, C. A., and Harpole, J. C., "Apollo Experience Report: Mission Planning for Apollo Entry," NASA TN-D-6725, 1972.
[18] Regan, F. J., and Anandakrishnan, S. M., *Dynamics of Atmospheric Re-Entry*, 1st ed., AIAA Education Series, AIAA, Washington, D.C., 1993, pp. 318–364.
[19] Powell, R. W., Striepe, S. A., Desai, P. N., Braun, R. D., Brauer, G. L., Cornick, D. E., Olson, D. W., Peterson, F. M., and Stevenson, R., "Program to Optimize Simulated Trajectories (POST) Utilization Manual," Vol. 2, Ver. 5.2, NASA Langley Research Center, Hampton, VA, 1997.
[20] Sutton, K., and Graves, R. A., Jr., "General Stagnation-Point Convective-Heating Equation for Arbitrary Gas Mixtures," NASA TR-R-376, Nov. 1971.
[21] Tauber, M. E., and Sutton, K., "Stagnation-Point Radiative Heating Relations for Earth and Mars Entries," *Journal of Spacecraft and Rockets*, Vol. 28, No. 2, 1991, pp. 40–42.
[22] Richardson, E. H., Munk, M. M., James, B. F., and Moon, S. A., "Review of NASA In-Space Propulsion Technology Program Inflatable Decelerator Investments," AIAA Paper 2005-1603, May 2005.
[23] Gnoffo, P. A., "Planetary-Entry Gas Dynamics," *Annual Review of Fluid Mechanics*, Vol. 31, Jan. 1999, pp. 459–494. doi:10.1146/annurev.fluid.31.1.459
[24] Humble, R. W., Lewis, D., Bissel, W., and Sackheim, R., *Liquid Rocket Propulsion Systems*, 1st ed., Chap. 5, Space Technology Series, McGraw–Hill, New York, 1995, pp. 272–279.
[25] Desai, P. N., Lyons, D. T., Tooley, J., and Kangas, J., "Entry, Descent, and Landing Operations Analysis for the Stardust Re-Entry Capsule," AIAA Paper 2006-6410, Aug. 2006.
[26] Brown, G. J., Epp, C., Graves, C., Lingard, J. S., and Darly, M., "Hypercone Inflatable Supersonic Decelerator," AIAA Paper 2003-2167, May 2003.
[27] Lyons, D., and Johnson, W., "Ballute Aerocapture Trajectories at Neptune," AIAA Paper 2004-5181, Aug. 2004.
[28] Kustas, F. M., Rawal, S. P., Willcockson, W. H., Edquist, C. T., Thornton, J. M., and Sandy, C., "Evaluation of High Temperature Multilayer Insulation for Inflatable Ballute," *Journal of Spacecraft and Rockets*, Vol. 38, No. 4, 2001, pp. 630–631.

C. Kluever
Associate Editor